jmb Article

Structural Insights into the Mechanism and Inhibition of the β-Hydroxydecanoyl-Acyl Carrier Protein Dehydratase from *Pseudomonas aeruginosa*

Lucile Moynié[1], Stuart M. Leckie[1], Stephen A. McMahon[1], Fraser G. Duthie[1], Alessa Koehnke[1], James W. Taylor[1], Magnus S. Alphey[1], Ruth Brenk[2], Andrew D. Smith[1] and James H. Naismith[1]

1 - Biomedical Sciences Research Complex, *The University, St. Andrews KY16 9ST, UK*
2 - Division of Biological Chemistry and Drug Discovery, *College of Life Sciences, University of Dundee, Dundee DD1 5EH, UK*

Correspondence to James H. Naismith: *naismith@st-andrews.ac.uk*
http://dx.doi.org/10.1016/j.jmb.2012.11.017
Edited by K. Morikawa

Abstract

Fatty acid biosynthesis is an essential component of metabolism in both eukaryotes and prokaryotes. The fatty acid biosynthetic pathway of Gram-negative bacteria is an established therapeutic target. Two homologous enzymes FabA and FabZ catalyze a key step in fatty acid biosynthesis; both dehydrate hydroxyacyl fatty acids that are coupled via a phosphopantetheine to an acyl carrier protein (ACP). The resulting *trans*-2-enoyl-ACP is further polymerized in a processive manner. FabA, however, carries out a second reaction involving isomerization of *trans*-2-enoyl fatty acid to *cis*-3-enoyl fatty acid. We have solved the structure of *Pseudomonas aeruginosa* FabA with a substrate allowing detailed molecular insight into the interactions of the active site. This has allowed a detailed examination of the factors governing the second catalytic step. We have also determined the structure of FabA in complex with small molecules (so-called fragments). These small molecules occupy distinct regions of the active site and form the basis for a rational inhibitor design program.

Introduction

In bacteria, plants and parasites, the synthesis of fatty acids is the result of the type II fatty acid synthetic system (often denoted FAS II). In contrast to the FAS I found in mammals, the FAS II pathway utilizes separate enzymes that catalyze the individual steps rather than a large multiprotein complex (for review, see Ref. 1). In the Gram-negative bacteria, two enzymes, FabA and FabB, are responsible for the production of unsaturated fatty acids. Unsaturated fatty acids are essential to the cells because it is the ratio of saturated/unsaturated fatty acids that controls the physical properties of the membrane.[2] The essential nature of unsaturated fatty acids has been demonstrated by making FabA (or FabB) deletion *Pseudomonas aeruginosa* mutant strains. The mutant strains are auxotrophic for unsaturated fatty acids under anaerobic conditions.[3,4]

FabA is a bifunctional enzyme that catalyzes the dehydration of hydroxyacyl-acyl carrier protein (ACP) to the *trans*-2-enoyl-ACP (Fig. 1a). This step is also catalyzed by the homologous FabZ enzyme. Uniquely, FabA can perform a second reaction, the isomerization of the double bond to a *cis*-3-decenoyl-ACP, although the *cis* product is formed only in small amounts. FabB specifically elongates this *cis*-unsaturated fatty acid in a process separate from the classic FAS II pathway. The *trans* fatty acid produced by both FabA and FabZ is reduced and subsequently elongated in the classic FAS II pathway.

Both FabA and FabZ have two principal catalytic residues, a His from one subunit and a carboxylic acid (Asp in FabA and Glu in FabZ) from the other. Although initial predictions suggested that the ability to catalyze the second step was related to the presence of Asp or Glu, a combined structural and functional study of FabZ of *P. aeruginosa* and FabA

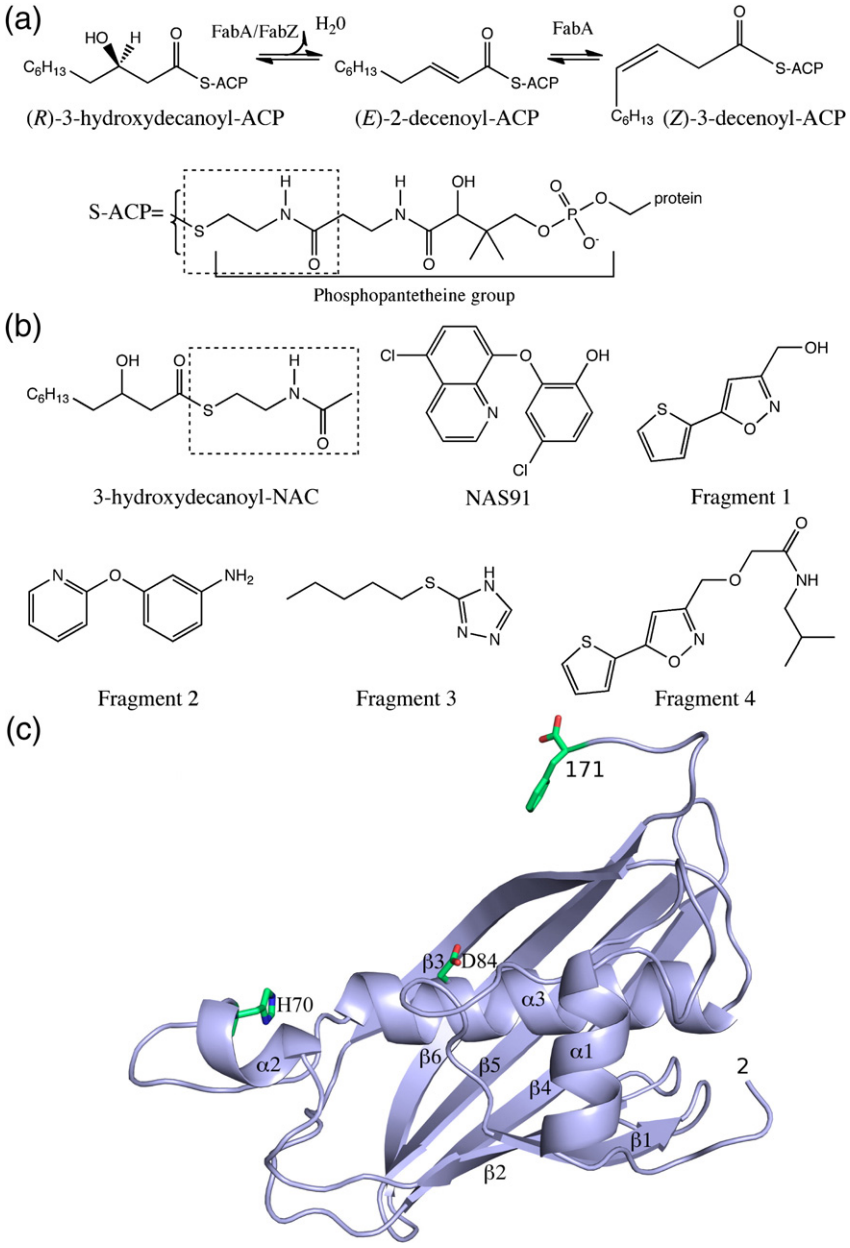

Fig. 1. Ligands of FabA. (a) Catalytic reaction of β-hydroxyacyl-ACP dehydratase; both FabA and FabZ catalyze the first reaction (dehydration) but only FabA catalyzes the second (isomerization). The chemical structure of the phosphopantetheine, the prosthetic group of ACP, is detailed. (b) Chemical structures of 3-hydroxydecanoyl-NAC that mimics the ACP substrate, *Pf*FabZ inhibitor NAS91 and *Pa*FabA binding fragments. The dashed boxes highlight the portion of the phosphopantetheine moiety mimicked by NAC. (c) Overall structure of *Pa*FabA monomer. The secondary structure elements are labeled; the two catalytic residues (H70 and D84) and the last phenylalanine (F171) have been added in stick (carbon atoms colored green, oxygen atoms colored red and nitrogen atoms colored blue).

of *Escherichia coli* demonstrated that the catalytic properties of the two enzymes are not related to a simple Asp/Glu switch. Rather, it was the shape of the substrate-binding pocket that underpinned the regioselectivity of the enzyme.[5,6] A structure of *Ec*FabA covalently bound (through the catalytic His residue) to the suicide inhibitor 2-decenoyl-*N*-acetylcysteamine (NAC) has been reported, but the inhibitor binds with a different stereochemistry than either substrates or products.[7] No structure of either FabA or FabZ in complex with a correctly configured substrate or substrate mimic has been reported, and this has hindered a full molecular understanding of the mechanism.

The increase in prevalence of antibiotic-resistant bacteria has meant that bacteria have re-emerged

as a significant problem in the developed world. It is generally accepted that there is a requirement for new drug starting points for novel targets. The significant differences between the human FAS I system and the type II system of bacteria, coupled to the essentiality of fatty acids in bacteria, have long made the type II pathway an antibacterial target.[8–10] Fragment-based approaches to devise new synthetic starting points for inhibitor design have become widely used in the pharmaceutical sector.[11,12] Fragment-based approaches rely on the identification of compounds that bind at the active site. Crucially, the compounds are synthetically simple; thus, they can be elaborated more easily than traditional drug starting points. Often, such fragments have very weak binding and, as a result of this, biophysical methods (e.g., NMR and crystallography) rather than assay screening are required to identify them.

We report the X-ray structure of the wild type of FabA of *P. aeruginosa* in the free form, in complex with four potential inhibitor starting points (so-called fragments) and the H70N mutant in complex with a substrate analogue: 3-hydroxydecanoyl-NAC. This first structure of a β-hydroxyacyl-ACP dehydratase in complex with a correctly configured synthetic substrate analogue rationalizes at a molecular level the catalytic mechanism of this bifunctional mechanism.

Results

Overall structure of *Pa*FabA

The crystal structure of the 171 residues of *Pa*FabA has been solved to a resolution of 2 Å. Residues 2–133 and 138–171 are well ordered. The monomer adopts the α+β "hotdog" fold previously described for the structure of *E. coli* FabA (*Ec*FabA),[7] a six-stranded antiparallel β-sheet wrapped around a long hydrophobic α-helix (α3) (Fig. 1c). Two other helices are also present on the structure: α-helix (α1) at the N-terminus and one small 3_{10} helix between β2 and β3 (α2). *Pa*FabA superposes with an rmsd of 0.58 for 166 C^{α} atoms to *Ec*FabA (68% sequence identity)[7] and an rmsd of 1.53 for 135 C^{α} to *Pa*FabZ[5] (31% identity for 133 residues).

In the native crystal, the only major differences between the 10 molecules of the asymmetric unit are in the C-terminal region. In chains B and E–J, interactions between Thr166 and Asp169 stabilize a type I turn, while in chains A, C and D, residues 165–168 form a type VIII turn (Fig. S2a). Despite this, the side chain of the terminal phenylalanine (Phe171) occupies approximately the same spatial position relative to the rest of structure and is stabilized by van der Waals interactions with Phe165 and Leu106. In effect, it acts as a "door" separating the active site from the ACP-binding groove (Arg104, Leu106, Gly107, Leu140, Gly163 and Phe165 from one monomer; Lys112, Phe114 and Ile134 from the other one). The same residue is found in *Ec*FabA, and although a different residue plays this role in FabZ proteins (Tyr88 in *Pa*FabZ or *Cj*FabZ and Tyr100 in *Hp*FabZ), the function is a conserved feature of the β-hydroxyacyl-ACP dehydratase family. For the activity of the protein, the C-terminal region needs to be flexible to allow access to the active site for the acyl-ACP substrate. The differences observed in the crystal may reflect this flexibility, as this region is also involved in the crystal packing, making it difficult to assign functional significance to these changes. The gel-filtration profile and crystal interfaces analysis (PISA[13]) confirm that the enzyme is a dimer (Fig. 2a). The two active-site residues (His70 and Asp84) have been confirmed by the observed loss of activity in the mutants H70N, D84N and H70N D84N.

Binding of 3-hydroxydecanoyl-NAC in the H70N *Pa*FabA

There are five monomers in the asymmetric unit; however, as they are essentially the same, we will describe only the most well ordered monomer (chain D) and its dimer with monomer C. The six C-terminal residues adopt a position similar to the conformation of chains A, C and D of the free structure (Fig. S2b). The rotamer of Phe171 adjusts due to contacts with the 3-hydroxydecanoyl-NAC, but it still blocks solvent access through the tunnel to the catalytic residues (Fig. S2b). 3-Hydroxydecanoyl-NAC is bound at the active site and makes contacts with both proteins in the dimer (Fig. 2a and b). The NAC group binds in the pantetheine tunnel, where it mimics the binding of pantetheine (Fig. 1). The pantetheine tunnel is formed by β3 of chain C and the loops between α2–α3 and β3–β4 from chain D. The NAC moiety makes hydrogen bonds to the carbonyl of Ala105 of chain C, and through a water molecule, it bridges to Met77, Val117 and Tyr155 from the other subunit (Fig. 2b and c).

The carbonyl of the thioester (C1) makes a hydrogen bond with NH of Ala105 of β3. Carbons C1–C4 of the 3-hydroxydecanoyl-NAC bind close to the catalytic residues Asp84 of the chain C and H70N from the chain D. The β-hydroxy interacts with the carboxylic group of Asp84 and a water molecule (denoted W1), which is hydrogen bonded to the amides of Cys80 and Gly79 from the other monomer (as well as to Asp84 from chain C). This water molecule is over 4 Å from H70 and conserved in the apostructure of FabA and FabZ. It had been proposed to occupy the position of the water eliminated from substrate.[5] The H70N mutation itself does not appear to change the protein structure or the arrangement of active-site residues; the side-chain atoms of Asn overlap with atoms of the His

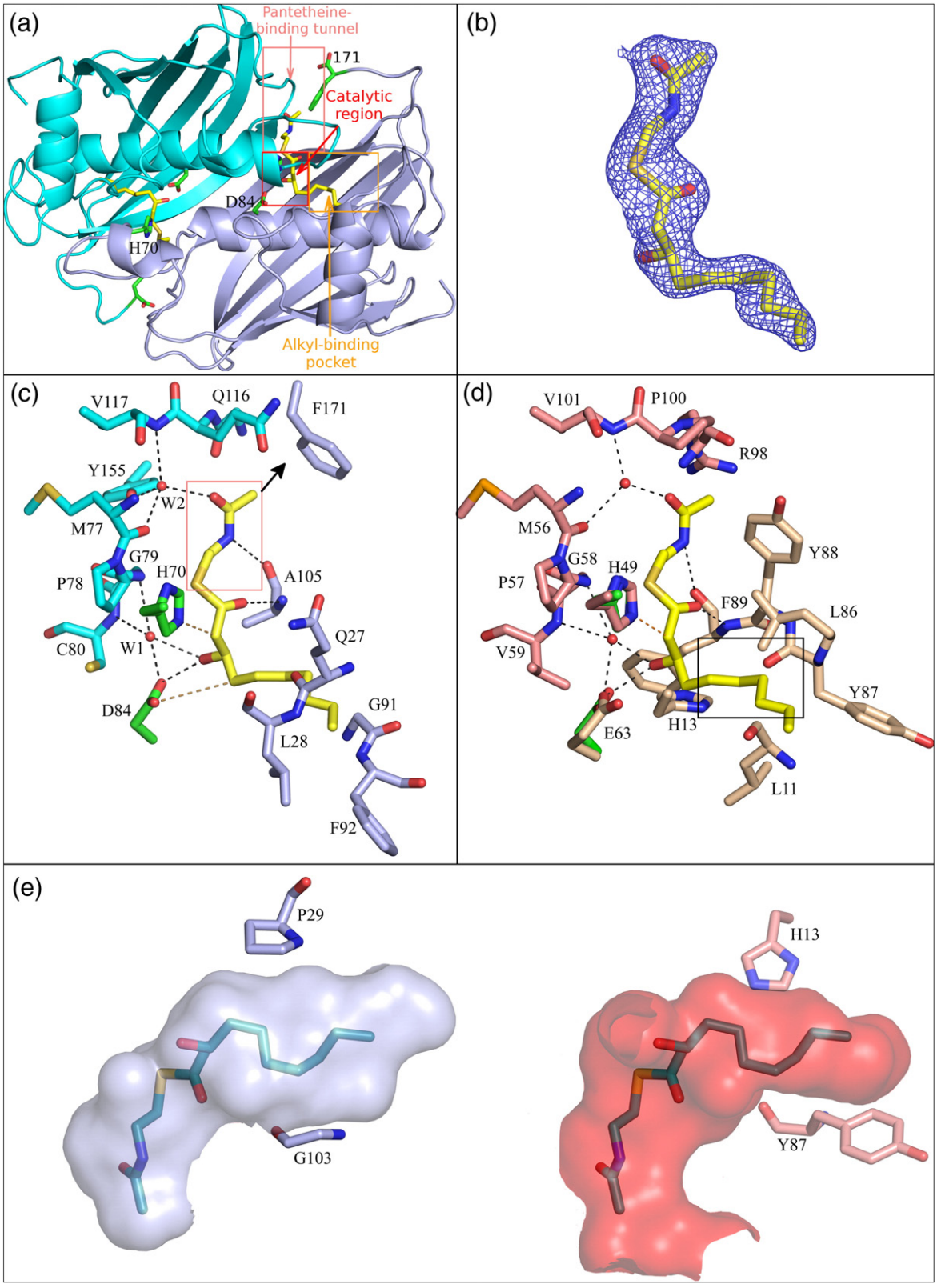

Fig. 2 (*legend on next page*)

side chain in the native structure (Fig. S3). The amide of the Asn side chain makes the same hydrogen bond to the carbonyl of Val76 as does $N^{\delta 1}$ of His70 in the wild type. Phe71 and Pro78 that stack against the imidazole ring of H70 are unchanged in the mutant, and the characteristic non-proline *cis*-peptide (residues 70–71) is preserved. Perhaps surprisingly, given its previously proposed role, W1 is unchanged in location or hydrogen bonding in the complex, except that it has an additional hydrogen bond, the 3-OH of the substrate mimic. Since W1 is beyond the normal range of van der Waals interactions with H70, we do not think that its preservation in the complex is a consequence of the H70N mutation. In the complex, there is an additional water molecule (Fig. S3) (which we denote W3), which may be present as a result of the mutation, but it only hydrogen bonds with W1 and D84 as well as H70N. We have made a model of the wild-type enzyme complex by simply changing H70N back to histidine. As a result, the N^{ε} of the histidine points directly to the C2 atom of the substrate mimic (Fig. 2c).

The aliphatic tail of 3-hydroxydecanoyl-NAC is embedded in a deep hydrophobic tunnel that is formed by α3, β3 and the loop connecting α1–β1. C4–C10 atoms of the lipid sit parallel with the α3 helix. A comparison of this complex with the covalent *Ec*FabA 2-decenoyl-NAC complex shows several differences (Fig. S4). The covalent bond between C3 of the 2-decenoyl-NAC and His70 results in the NAC group being pushed further along the groove away from the active site while the aliphatic tail is pulled in toward the active site relative to the complex described here. Consequently, the critical C1–C4 atoms of the lipid that undergo chemical transformation are misaligned between the two structures (Fig. S4). As a result, the interactions between the catalytic residues and the lipids are very different.

Comparison of *Pa*FabA and *Pa*FabZ

As expected, *Pa*FabA and *Pa*FabZ adopt the same fold. The β-sheet of the two proteins superposes quite well; however, the helix α1, the end of the strand β1, the beginning of the strand β3 and the orientation of helix α3 are shifted. The positions of loops α1–β1, β1–β2, α3–β3 and β4–β5 are different due to sequence insertions in the *Pa*FabA protein (Fig. S1). Comparison of the structure around the active site shows that the pantetheine-binding tunnel is similar. In the catalytic region, the histidines (70 and 49 for *Pa*FabA and *Pa*FabZ, respectively) are essentially in the same position but a glutamate replaces the aspartate in FabZ proteins. However, a compensating shift in helix α3 (which moves away from the active site in *Pa*FabZ) means that the net shift in the relative positions of the carboxylate groups is very small (approximately 1.2 Å) (Fig. 2d and Fig. S5), consistent with the previous observation that the Glu/Asp substitution has no effect on the catalytic ability.[5] Two residues adjacent to the catalytic machinery, Ala66 and Phe89 of *Pa*FabZ, are replaced in *Pa*FabA by Trp87 and Ala105, respectively. The double mutation can be seen as partially compensating in that the phenyl ring in *Pa*FabZ overlaps with the indole of Trp87 *Pa*FabA (despite the side chains coming from different regions of structure).

As outlined first by Kimber *et al.*, there are major differences in the alkyl-binding pocket that are clearly visualized by this new complex of *Pa*FabA.[5] Around the C4 and C5 atoms, in *Pa*FabA, the distance between Pro29 and Arg104 on opposite sides of the active site is over 10 Å, whereas in *Pa*FabZ, His13 and Tyr88 are 7.8 Å apart. The main chain of Tyr87 in *Pa*FabZ is displaced into the active site such that it would clash with C6 and C7 of the ligand (Fig. 2d and e). These changes are a result of differences in the loop structures connecting α1–β1 and α3–β3 in the two proteins. In all FabA proteins, the α1–β1 loop is conserved and is larger than observed in FabZ sequences. In the FabA structures (both *Pa*FabA and *Ec*FabA), this loop contributes extensively to the alkyl-binding tunnel while the conserved α3–β3 (shorter than FabZ sequences) plays a minor role. In FabZ, the larger α3–β3 loop

Fig. 2. Structural biology of FabA. (a) Overall structure of *Pa*FabA dimer. The active site is formed by the dimer; the two key catalytic residues (H70 and D84) come from different monomers that form the dimer. The C-terminal phenylalanine and the 3-hydroxydecanoyl-NAC are shown in stick. The three regions of the active site, the pantetheine-binding tunnel, the catalytic region and the alkyl-binding pocket, have been indicated by boxes. (b) Final $2F_o - F_c$ electron density at 1 σ around the 3-hydroxydecanoyl-NAC in complex with *Pa*FabA H70N. (c) Interactions between the 3-hydroxydecanoyl-NAC (yellow) and the active-site residues of *Pa*FabA with His70 modeled (experimental structure has H70N mutation). Residues within 4.0 Å of the fragments are displayed, and hydrogen bonds are shown as black broken lines. The two catalytic residues are correctly positioned for proton transfer, represented by sand-colored broken lines. The pantetheine-binding tunnel is highlighted by a box and an arrow. (d) Superposition of C1–C4 portion of 3-hydroxydecanoyl-NAC *Pa*FabA complex (carbons shown as yellow stick) onto *Pa*FabZ (carbons from the two monomers that form the *Pa*FabZ active site are colored pale orange and pale pink) does not give any clashes and would give a complex capable of catalyzing the dehydration reaction. The differences in the alkyl-binding pocket would, however, result in clashes with carbons C5–C8 (black box) of substrate and *Pa*FabZ. The catalytic residues of *Pa*FabA are shown with carbons colored green. (e) Surfaces of the active site of *Pa*FabZ (red) and *Pa*FabA (light blue) have been represented. The carbons of the 3-hydroxydecanoyl-NAC have been shown in teal. Amino acids of *Pa*FabZ that narrow the alkyl tunnel (H13 and Y87) are drawn in stick.

contributes extensively to the alkyl-binding tunnel and the shorter α1–β1 plays only a minor role. These changes are accompanied by a shift of the N-terminus of β3 that shifts into the alkyl-binding tunnel in *Pa*FabZ when compared to *Pa*FabA (Fig. S5).

Discovery of binding fragments

A screen of 436 compounds from the Maybridge Ro3 500 fragments library was conducted using saturated transfer difference and water logsy NMR techniques. We identified 39 fragments as potentially binding to *Pa*FabA, and we have been able to obtain three co-complexes (Fig. S6a–c). 5-(2-Thienyl)-3-isoxazolyl methanol (fragment 1) binds in the pantetheine-binding tunnel occluding it (Fig. 3a and Fig. S6d). The thienyl group displaces the C-terminal Phe171 residue and makes extensive van der Waals interactions. The displacement of Phe171 results in a rearrangement of six C-terminal residues (Fig. S2c). The isoxazolyl ring interacts with the protein via a conserved water molecule, and the methanol group hydrogen bonds to NH of Gly79. 3-(Pyridin-2-yloxy)aniline (fragment 2) binds at the catalytic site (Fig. 3b and Fig. S6e), the pyridine ring overlapping with the methanol of fragment 1. The N atom of the pyridine ring forms a hydrogen bond with Ala105, and the aniline ring fills the C4 to C6 substrate binding pocket of the protein. The amide group points into the empty hydrophobic tunnel. Gln88 adopts a second partially occupied conformer, which results in contacts with the aniline ring. 3-(Pentylthio)-4*H*-1,2,4-triazole (fragment 3) is quite similar to the substrate and overlaps with fragment 2. The triazole ring occupies the same space as the pyridine ring of fragment 2 and makes a bidentate hydrogen bond to Ala105 (Fig. 3c and d and Fig. S6f). The hydrophobic tail reaches into the hydrophobic alkyl chain tunnel. The thioether group does not displace the water molecule bound to Asp84. This fragment complex was obtained by soaking, and the density is less well ordered than the other two. Fragment 4, the *N*-isobutyl-2-([5-(2-thienyl)-1,2-oxazol-3-yl]methoxy)acetamide, has been identified by virtual screening based on fragment 1. In the crystal structure, one molecule binds in the pantetheine-binding tunnel of monomer B (Fig. 3d). The thienyl and the oxazole rings have reversed compared to fragment 1, and the *N*-isobutyl-acetamide group extends to the ACP-binding groove, making a

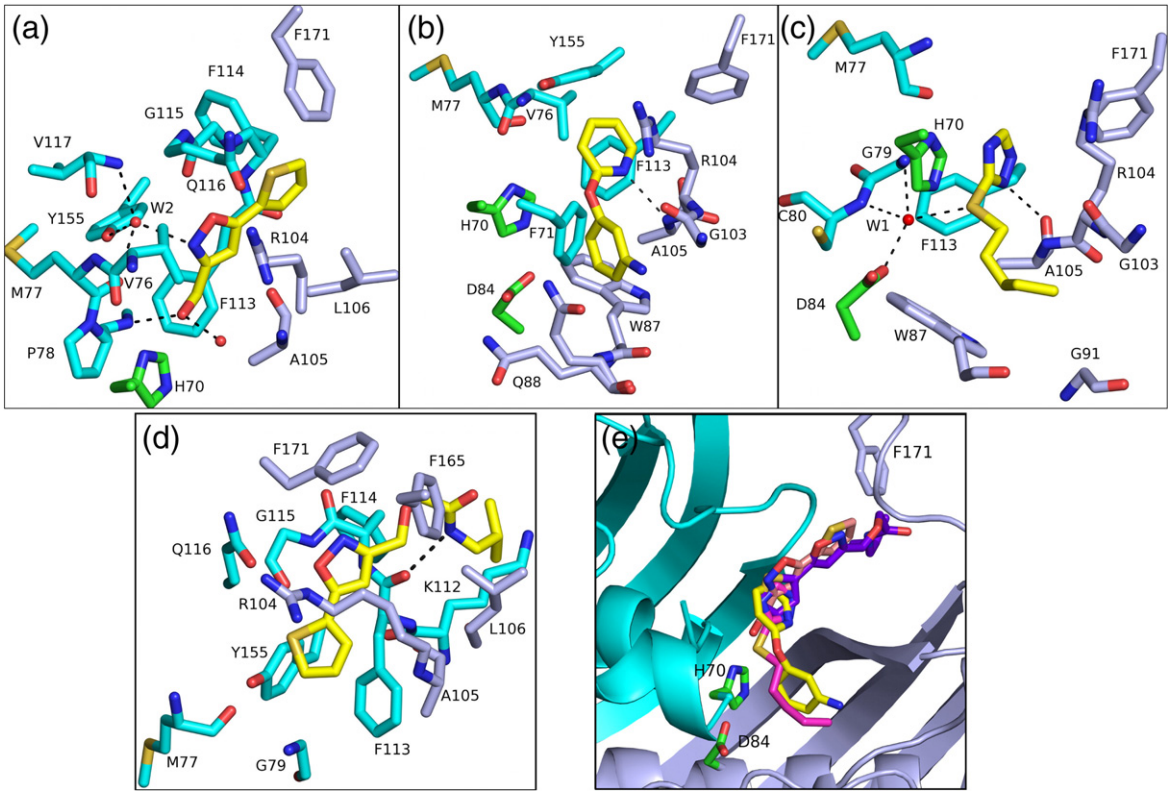

Fig. 3. Crystal structures of *Pa*FabA complexes with different fragments. Interactions between fragments 1 (a), 2 (b), 3 (c) and 4 (d) with *Pa*FabA are shown. Residues within 4.0 Å of the fragments are displayed. A change in orientation of the figures has been made to allow visualization of the interactions between the fragments and enzyme more clearly. Fragments 2 and 3 bind at the catalytic region while fragments 1 and 4 occlude the pantetheine-binding tunnel (e). A superposition shows that the four fragments occupy different portions of the binding site.

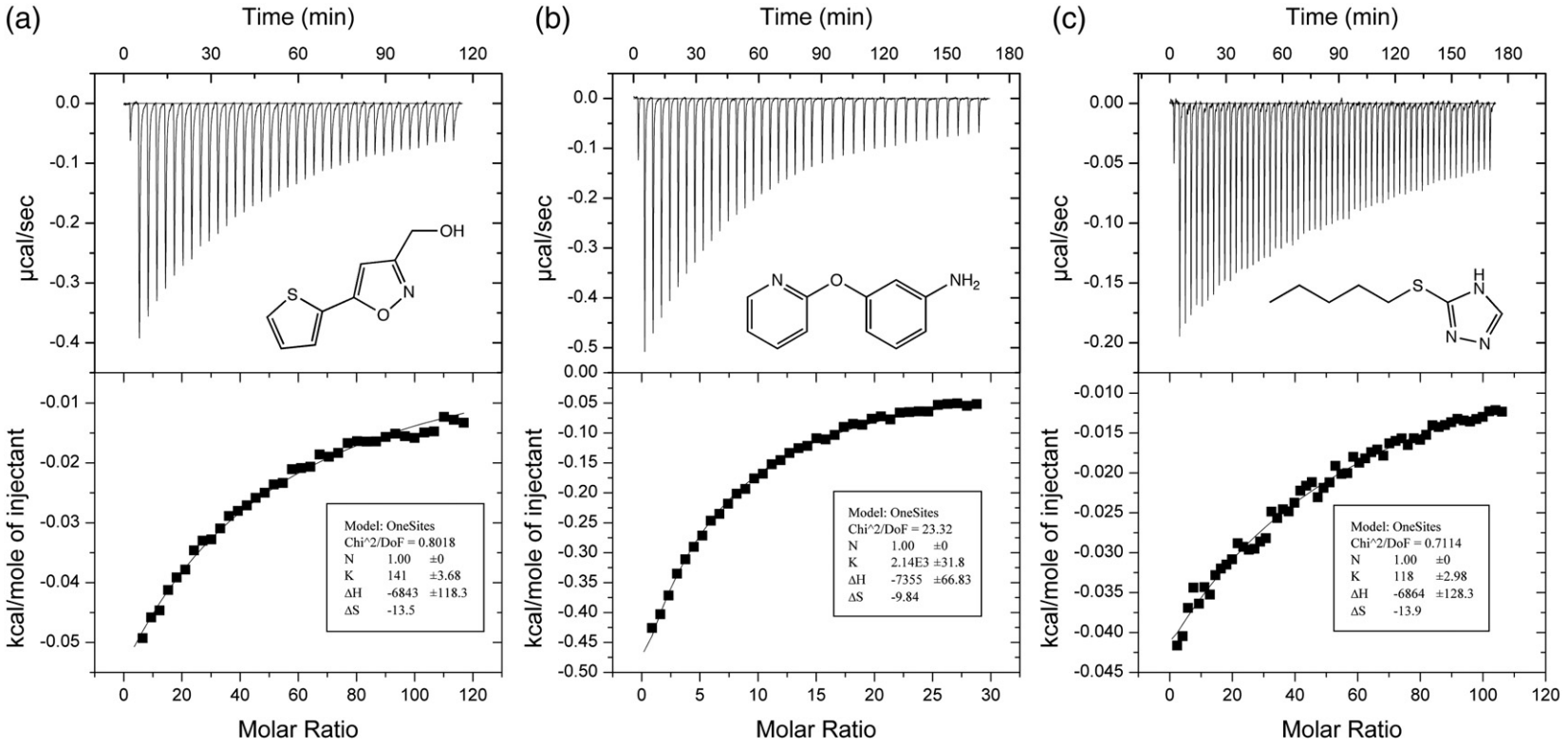

Fig. 4. Isothermal calorimetry titration of fragments 1 (a), 2 (b) and 3 (c) with *Pa*FabA. Upper panel: raw titration data. Low panel: integrated and dilution corrected peak areas of the raw data. Data were fitted with a single-binding-site model to evaluate the dissociation constant (K_d).

hydrogen bond with the main chain of Phe113. Analysis of the binding of the fragments by isothermal titration calorimetry shows a binding constant of around 10 mM for fragments 1 and 3 and 0.5 mM for fragment 2 (Fig. 4); fragment 4 was too insoluble to be measured. Surface complementarity[42] analysis has been used to quantify the fit of ligands to protein pockets and is therefore useful in evaluating fragment for suitability for further development. Such analysis shows that fragment 2 has almost a perfect score of 0.93 (on a scale of 0 to 1), and the other fragments score between 0.35 and 0.58 consistent with our biophysical data.

Discussion

The enzymes of FAS II pathway are established targets for antibacterial drugs, although recent works suggest that their applicability may be limited to Gram-negative organisms.[8–10,14] Inhibitors have been reported for FabZ from two organisms *Helicobacter pylori* and *Plasmodium falciparum*.[10,15,16] Similar progress has not been reported for FabA (the covalent configured 2-decenoyl-NAC cannot adopt a configuration that matches the substrate), yet FabA is a particularly attractive target since its isomerization activity, which is essential, is not possessed by FabZ (whereas FabA possesses the dehydration activity of FabZ, potentially allowing FabA to compensate for loss of FabZ). The discovery of binding fragments that occupy multiple different positions in the *Pa*FabA active site serves as a starting point for inhibitor design (Fig. 3e). Fragments 1 and 4 block the pantetheine-binding tunnel and thus partly mimic the flavonoids and synthetic inhibitors reported for *Hp*FabZ[15,17–19] (Fig. S7b). However, in *Hp*FabZ, both flavonoids and synthetic inhibitors extend to a groove around the pantetheine-binding tunnel; this groove does not exist in *Pa*FabA as it is filled by the side chain of the conserved Arg104 (found also as lysine). Thus, subtle differences in the pantetheine-binding tunnel are reflected in the binding of inhibitors. Fragment 2 has some similarity with NAS91, 4-chloro-2-[(5-chloroquinolin-8-yl)oxy]phenol, a competitive inhibitor of *Pf*FabZ, in that both contain two aromatic rings link by an oxygen atom[16] and both bind in a broadly similar location. Unlike NAS91, however, fragment 2 does not interact with the catalytic residues. The difference in binding observed between the two compounds reflects the shift of the α3 helix between the structures (Fig. S5). Fragment 3 is the first compound reported that occupies the alkyl-binding tunnel.

The substrate complex of *Pa*FabA allows the mechanism to be described in molecular detail (Figs. 2c and 5a and b). His70 from one subunit is positioned to abstract the proton from C2 while Asp84 from the other subunit is directly hydrogen

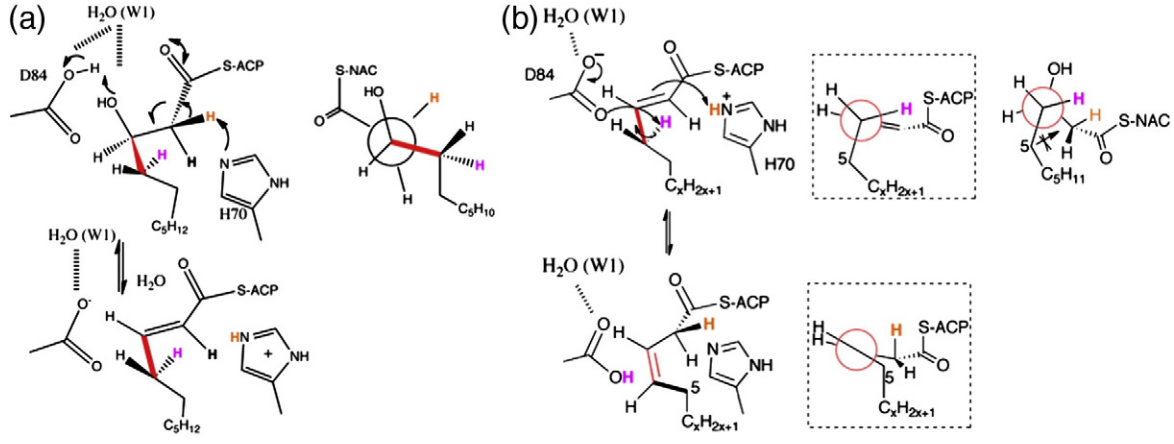

Fig. 5. Catalytic mechanism. (a) The common dehydration mechanism of FabA and FabZ. Both the C3 hydroxyl and C2 proton (orange) are abstracted from the same face according to labeling studies. The catalytic residues for *Pa*FabA are shown. In *Pa*FabZ, the equivalent residues occupy essentially identical positions, although a Glu replaces the Asp. On the right-hand side, the conformation of 3-hydroxydecanoyl-NAC found in the structure is shown and is consistent with the suprafacial elimination of water. W1 is shown as part of the hydrogen bond network around Asp84. It may assist in setting the protonation state of Asp84 or it could take part in the shuttling of protons between this residue and the substrate. (b) FabA catalyzes the isomerization by extracting the *pro*-R proton (purple) from C4 of its substrate. Shown boxed in the middle column are projections of the natural enzyme substrate. On the right, the conformation of 3-hydroxydecanoyl-NAC found in the structure does position the *pro*-R proton for abstraction and would lead to a *cis* configuration of the C3–C4 bond (red). Thus, the complex serves as valid model for the second reaction. The position of the C5 is critical. In *Pa*FabZ, which does not catalyze isomerization, the different protein structure would result in clashes with C5 and C6 of substrate thus preventing C5–C4–C3–C2 adopting the +60° configuration required to form a *cis* C3–C4 double bond.

bonded to the (*R*)-configured C3 hydroxyl, with a water molecule (W1) involved in the network (Fig. 2c). In an (*S*)-enantiomer, the hydroxyl would point away from Asp84 (Fig. 5a), explaining the stereoselectivity of the dehydration. Chemical reasoning implies that protonation of the hydroxyl would be required for elimination; therefore, a proton must be supplied by the protein. We suggest that the most likely candidate is OD1 of Asp84, although a protonated Asp would be unusual at physiological pH. Asp84 sits in an extensive hydrogen bond network involving W1 inside a hydrophobic active site; we hypothesize that this could shift the effective pK_a but direct evidence is lacking. In this model, W1 does not arise from elimination from the substrate as previously suggested[5]; rather, it plays a role in mediating a complex network of hydrogen bonds (W3 plays no role). The substrate dihedral angle C1–C2–C3–C4 at 152° is very close to the expected *trans* (180°) configuration of the resulting product; as a result, the substrate is bound in a conformation preset for E1cB-type elimination and formation of the *trans* C2–C3 product. In this structural arrangement, the net proton transfer (from C2 to the hydroxyl) is suprafacial, in agreement with labeling studies on the reverse reaction[20] (Fig. 5a).

The second step, uniquely catalyzed by FabA, is the isomerization of substrate from *trans* C2–C3 to *cis* C3–C4. In FabA, the newly deprotonated Asp84 is 4.1 Å from C4 of the substrate mimic; thus, only a small movement of the C4 atom would be needed for Asp84 to deprotonate C4 (Fig. 5b), forming an allyl anion. In the substrate mimic complex, the *pro*-R hydrogen on the C4 atom points toward Asp84, consistent with deuterium incorporation experiments showing the *pro*-R, which is extracted.[20] The substrate mimic has a dihedral angle C2–C3–C4–C5 of +60°. In the true substrate, this configuration would result in the *cis*-configured C3–C4 double bond (Fig. 5b) (upon quenching of the allyl anion by protonation at C2). An alternate C2–C3–C4–C5 conformer (−60°) of the substrate mimic is not possible in the active site, as it would result in C5 clashing with the catalytic Asp84 (or Glu63 in *Pa*FabZ). Even if such a clash could be accommodated, the proton on C4 would be too far from the carboxylate of Asp84 to be extracted. (The significance of such a −60° configuration is that, in the substrate, it would lead to a *cis*-configured C3–C4 double bond.) The third conformer (180° that leads to a *trans* C3–C4) is impossible as it would result in severe (interpenetrating) clashes of C6 and C7 with α3 helix in both *Pa*FabA (and *Pa*FabZ).

An important question is why does *Pa*FabZ not catalyze the second isomerization step? The location of C2 and C3 of the substrate will be the same in both enzymes, their position determined by the chemical requirement for proton transfer and dehydration involving the conserved histidine and glutamic (aspartic) acid residues. As dehydration by FabZ also gives the *trans* C2–C3 product, the C4 position is therefore expected to be located close to the C4 position reported for the substrate mimic complex. Superposition of the *Pa*FabA complex with *Pa*FabZ shows that C1–C4 atoms of the substrate mimic do not clash with the *Pa*FabZ (Fig. 2d) and are setup for catalysis. Our structural data identify two key spatial considerations for isomerization. Firstly, the C4 atom must be positioned such that the catalytic carboxylic acid (Asp84) can abstract the *pro*-R proton to form the allyl anion, and secondly, the C5 atom must have enough space for the substrate to adopt a dihedral C2–C3–C4–C5 angle of +60°. The superposition of *Pa*FabA complex with *Pa*FabZ structure shows that the C5 of substrate would clash with the side chain of His13 of *Pa*FabZ (2.9 Å) and that C6 would clash with the backbone carbonyl of Tyr87 (2.2 Å). These clashes would prevent C5 in the substrate from adopting +60° required for the *cis* configuration (the *trans* configuration would also be forbidden). The clashes result from changes in the hydrophobic tunnel formed by the loop connecting α1–β1 and the shift of β3. His13 is conserved in most FabZ (Asn in some lactobacillales bacteria), whereas in FabA proteins, a conserved proline (Pro29) is found in this position (Fig. 2e). Single-site mutation *Ec*FabZ-H13P or *Ec*FabA-P29H does not remove or confer isomerization activity.[5] Domain swaps of two very closely related *Enterococcus faecalis* proteins FabN (which unusually has FabA-like activity despite being more closely related to FabZ in sequence terms) and FabZ[6] identified a chimera capable of isomerization.[6] In the active chimeric protein, β3–β4 from *Ef*FabN was placed in *Ef*FabZ. Single-site mutants failed to achieve the same effect, consistent with the complex structure showing that the main chain at Tyr87 (located on β3 in *Pa*FabZ), not simply side chain at His 13, is involved in blocking C5 from adopting the +60° configuration.

Conclusion

FabA is a bifunctional enzyme and an attractive antibiotic target for pathogenic Gram-negative organisms. By solving the structure of *Pa*FabA in complex with a substrate mimic, we have provided molecular insight into the catalytic mechanism of this enzyme. This new structure supports the hypothesis that differences in the alkyl-binding site between FabZ and FabA, rather than changes in catalytic residues, are responsible for the fate of the substrate in these enzymes. We have identified and described four fragment complexes that may serve as starting points for future inhibitor design. One fragment has submillimolar affinity and appears a very good match to the substrate-binding pocket.

Materials and Methods

Materials

NAC, 4-dimethylaminopyridine and 3-ethyl-1-(3-dimethylaminopropyl)carbodiimide hydrochloride were purchased from Sigma-Aldrich; *trans*-2-decenoic acid was from TCI, and (±)-3-hydroxydecanoic acid was from Wako Chemicals.

Synthesis of 3-hydroxydecanoyl-NAC thioester

The substrate analogue is synthesized using a published procedure by coupling the corresponding carboxylic acid with NAC.[21,22]

Cloning and purification of *Pa*FabA

*Pa*FabA was cloned with an N-terminal tobacco etch virus protease cleavable His_6-tag in pDEST14 vector using a modified version of Gateway cloning system.[23] Mutations H70N, D84N and H70N D84N were constructed with a modified protocol of the QuikChange method[24,25] using the primers 5′-TTC-GCC-TGT-AAC-TTC-GAA-GGC-GAT-CCG-GTC-ATG and 5′-GAA-GTT-ACA-GGC-GAA-GAA-CCA-CAG-GTC-CGG-GTT for H70N mutation and 5′-GCC-TGA-ATG-CCA-TGT-GGC-AGC-TGG-TCG-GT and 5′-CAT-GGC-ATT-CAG-GCC-CAG-GCA-ACC-GGG-C for D84N mutation. Mutations were confirmed by sequencing. Wild-type protein was over-expressed in *E. coli* Tuner (DE3) cells. Cells were grown at 37 °C in LB medium containing 100 μg ml^{-1} ampicillin until an OD_{600} of 0.6 was reached and then induced with 0.4 mM IPTG at 15 °C overnight. Mutant proteins were expressed in BL21 STAR cells with autoinduction media[25] at 20 °C for 48 h and purified as the wild type. Harvested cells were re-suspended in lysis buffer [20 mM $NaHPO_4$ (pH 7.4), 10 mM imidazole and 500 mM NaCl] and incubated at room temperature for 1 h with 100 μg ml^{-1} lysozyme and 20 μg ml^{-1} DNase. This was followed by two passes through a cell disruptor (Constant Systems) and centrifugation for 30 min at 75,500***g***. The supernatant was applied to a charged HisTrap Nickel Sepharose, high-performance column (GE Healthcare) (immobilized metal ion affinity chromatography) and washed with lysis buffer containing 30 mM imidazole, and protein was eluted with lysis buffer containing 300 mM imidazole. The imidazole was removed by desalting chromatography before adding the tobacco etch virus protease to cleave the His_6-tag. Protein was applied to a second immobilized metal ion affinity chromatography column followed by Superdex S75 gel-filtration chromatography (GE Healthcare) equilibrated with 10 mM Tris (pH 7.5), 150 mM NaCl and 10% glycerol. Protein fractions were pooled and concentrated to 8 mg ml^{-1}, purity was judged by SDS gels and the identity was confirmed by mass spectrometry.

Identification of binding fragments by NMR

Binding fragments were identified by screening a Maybridge Ro3 500 fragments library by saturated transfer difference and water logsy NMR techniques.[26,27] The soluble fragments with a clear spectrum (436) were organized into 54 cocktails of 8 fragments and 1 cocktail of 4 fragments such that spectra of individual compounds could be identified. FabA was diluted to a final concentration of 20 μM in 50 mM sodium phosphate (pH 7.5), 10% D_2O and the fragment cocktail added to a final concentration of 1 mM. The total volume of the experiment was 750 μl. Using a Bruker Avance 500, we performed the two NMR experiments sequentially on each sample. Data were processed with Topspin 2 and AMIX to identify fragments binding.

Crystallization and structure determination

Crystals of the wild-type *Pa*FabA appeared at 20 °C after 2 days of incubation from a mixture of 1 μl of protein solution (8 mg ml^{-1}) with 1 μl of reservoir solution containing 18% polyethylene glycol (PEG) 3350, 0.12 M sodium potassium phosphate, 6.4% hexanediol and 0.1 M sodium citrate (pH 4.5) in a sitting-drop vapor diffusion experiment. Crystals were cryoprotected by supplementing the mother liquor with 15% glycerol. Prior to crystallization, 1 mM 3-hydroxydecanoyl-NAC was incubated with the H70N mutant at 8 mg ml^{-1} for 1 h and crystals appeared after 1 day by mixing 2 μl of protein solution with 1 μl of 13% PEG monomethyl ether 5000, 0.1 M sodium citrate (pH 4.5) and 0.09 M lithium sulfate again in a sitting-drop vapor diffusion experiment. Co-crystallization and soaking of fragments were conducted in two steps. The 49 hits were arranged into cocktails of four fragments each at 12.5 mM. Those that gave strong additional density either by soaking or by co-crystallization were repeated with individual compounds. Crystals of wild type with [5-(2-thienyl)-3-isoxazolyl] methanol (fragment 1) and *N*-isobutyl-2-([5-(2-thienyl)-1,2-oxazol-3-yl]methoxy)acetamide (fragment 4) were obtained by co-crystallization under the same condition as the 3-hydroxydecanoyl-NAC complex. Co-crystals with 3-(pyridin-2-yloxy)aniline (fragment 2) were obtained by mixing 2 μl of protein solution with 1 μl of the reservoir solution with 15% PEG 8000, 0.2 M magnesium chloride and 0.1 M Tris–HCl (pH 8.0). Crystals complexed with 3-(pentylthio)-4*H*-1,2,4-triazole (fragment 3) were obtained by soaking wild-type crystals for 20 min with mother liquor containing 12.5 mM compound before cryoprotection. Data were collected at beamlines ID29 at the European Synchrotron Radiation Facility and IO2 and IO4-1 at the Diamond Light Source Oxfordshire or in-house using a Rigaku Micromax™-007HF Cu anode with VariMax optics and a Rigaku Saturn 944 + CCD detector. Data were processed with HKL2000[28] or Xia2.[29–33] The native structure was solved using *Ec*FabA as a model[7] with the program MOLREP.[34] Complex structures were solved using the coordinates of the wild-type *Pa*FabA and the program Phaser.[35] PHENIX[36] was used for autobuilding from molecular replacement solutions. Models were adjusted with Coot[37] after each round of refinement in REFMAC5.6 from the CCP4 program suite 6.2.0 with local NCS restraints (option in program) and TLS parameters[38] applied throughout for all structures. The native structure contains 10 molecules in the asymmetric unit. One molecule of glycerol and a phosphate ion are present in each active site. Judging by average *B*-factor, subunits C, E and G are the most well ordered. There are five

molecules in the asymmetric unit of the 3-hydroxydecanoyl-NAC complex; one molecule of 3-hydroxydecanoyl-NAC is present in each active site and was assigned an occupancy of 1 (we did not have sufficient resolution to confidently refine occupancy). The ligands in chains B and C are in well-defined electron density. The ligand can be modeled in the other monomers; however, the density is less well defined. Co-complex crystals with fragments 1, 2 and 3 contain 20, 2 and 5 protein monomers in the asymmetric unit, respectively. Again, each active site was built with a fragment with occupancy of 1 as difference density was visible in each. Chains D, F, J and N for fragment 1; chain B for fragment 2; and chains B and E for fragment 3 have the clearest density for the ligand. The structure with fragment 4 contains five molecules in the asymmetric unit but, only in chain B, was the electron density clear enough to model a bound fragment (in the pantetheine-binding tunnel). In chains A and E, there is additional density at the active site, but we have been unable to model this satisfactorily. Final refinement statistics are given in Table 1. Atomic coordinates and structure factors have been deposited in the Protein Data Bank (4FQ9, 4B0I, 4B0J, 4B0B, 4B0C and 4B8U). Coordinates and topologies of ligands were generated by PRODRG.[39] The qualities of all structures were checked with MolProbity.[40] Figures were drawn using PyMOL.[41]

Enzyme assays

Activity was assessed by a spectrophotometry assay based on the absorbance of the (*E*)-2-decenoyl-NAC at 260 nm.[42] Briefly, 0.3 mM 3-hydroxydecanoyl-NAC was solubilized in sodium phosphate (pH 7.5). The reaction is started by adding 14 μg ml^{-1} of protein, and the increase of the absorbance is monitored at 30 °C. This assay is not suitable to assess the inhibition of the fragments because they absorb at this wavelength.

Isothermal microcalorimetry titration

The affinities of ligands 1, 2 and 3 were measured by isothermal titration calorimetry using a VP-ITC instrument (GE Healthcare) at 20 °C. Titrations were performed using 37×7.5 μl injections of 30 mM fragment 1 in 55 μM *Pa*FabA or 4 mM fragment 2 in 32 μM proteins or 57×5 μl injections of the fragment 3 at 25 mM in 50 μM *Pa*FabA in the same buffer [100 mM sodium phosphate

Table 1. Crystallographic data and refinement statistics

	*Pa*FabA	H70N–3-OH-decanoyl-NAC complex	Fragment 1 complex	Fragment 2 complex	Fragment 3 complex	Fragment 4 complex
Data collection						
Space group	*C*2	$C222_1$	$P2_1$	$P2_12_12$	*C*2	*C*2
Cell dimensions						
a, *b*, *c* (Å)	146.8, 135.8, 111.0	110.8, 169.7, 108.3	109.8, 108.2, 202.3	59.3, 118.0, 48.0	114.9, 141.7, 78.9	113.9, 143.7, 78.0
α, β, γ (°)	90, 108.8, 90	90, 90, 90	90, 103.13, 90	90, 90, 90	90, 115.7, 90	90, 116.5, 90
Resolution (Å)[a]	50–2.02 (2.07–2.02)	54–2.03 (2.15–2.03)	24–2.5 (2.54–2.5)	37–1.9 (1.95–1.9)	35–2.7 (2.77–2.7)	72–2.76 (2.83–2.76)
R_{merge}	0.082 (0.477)	0.057 (0.457)	0.109 (0.371)	0.106 (0.361)	0.044 (0.713)	0.081 (0.415)
$I/\sigma(I)$	8.5 (2.3)	15.23 (2.7)	13.6 (2.3)	14.9 (4.5)	16.8 (2.2)	7.5 (2.0)
Completeness (%)	98.6 (98.3)	98.0 (99.5)	96.9 (84.3)	99.0 (97.6)	99.2 (99.6)	96.8 (98.8)
Average redundancy	3.2 (2.9)	4.5 (4.5)	3.4 (2.6)	7.8 (4.4)	3.9 (4.0)	3.0 (3.1)
Z′	10	5	20	2	5	5
Refinement						
Resolution (Å)	50–2.02	54–2.03	24–2.5	37–1.90	35–2.7	72–2.76
No. of reflections	126,685	61,486	147,156	25,582	29,525	26,426
R_{work}/R_{free}	0.19/0.21	0.17/0.20	0.23/0.26	0.20/0.23	0.20/0.23	0.18/0.22
No. of atoms						
Protein	13,136	6490	25,965	2646	6494	6431
Water molecules	721	355	839	299	20	25
Compound	122	95	240	28	55	25
B-factors ($Å^2$)						
Protein	35.6	53.9	49.6	24.0	67.3	64.9
Chain B range	30.8–41.9	51.4–61.2	44.6–54.9	23.8–24.2	60.4–79.7	58.7–75.2
Water	42.0	57.5	46.5	33.2	55.9	57.6
Compound	47.1	69.5	57.7	29.1	88.2	68.3
Compound B range	29.2–59.5	60.9–84.6	49.6–73.6	29.1–29.1	84.91–91.8	—
rmsd						
Bond lengths (Å)	0.009	0.011	0.009	0.012	0.011	0.011
Bond angles (°)	1.49	1.275	1.335	1.254	1.453	1.385
Summary of the Ramachandran plots (%)[b]	98.51/1.49/0	98.20/1.68/0.12	97.42/2.58/0.0	97.91/2.09/0	97.46/2.54/0	98.29/1.71/0

The range of temperature factor is shown for the ligands within the asymmetric unit (highest in structure to lowest in structure).
[a] Numbers in parentheses represent statistics in highest-resolution shell.
[b] Percentages of residues in the most favored regions/allowed regions/disfavored regions.

(pH 7.00) containing 10% dimethyl sulfoxide]. Experiments were limited by the solubility of fragments, and the affinity of fragment 4 cannot be estimated by this method. The heats of dilution measured from injection of the ligands into the buffer were subtracted from the experimental data, and titration curves were fitted into a single-site binding using the Origin software.

Acknowledgements

The research leading to these results has received funding from the European Community's Seventh Framework Programme (FP7/2007–2013) under grant agreement number 223461.

Supplementary Data

Supplementary data to this article can be found online at http://dx.doi.org/10.1016/j.jmb.2012.11.017

Received 3 September 2012;
Received in revised form 12 November 2012;
Accepted 13 November 2012
Available online 19 November 2012

Keywords:
fatty acid biosynthesis;
β-hydroxydecanoyl-ACP dehydratase;
bacterial virulence

Abbreviations used:
ACP, acyl carrier protein; NAC, *N*-acetylcysteamine; PEG, polyethylene glycol.

References

1. White, S. W., Zheng, J., Zhang, Y. M. & Rock (2005). The structural biology of type II fatty acid biosynthesis. *Annu. Rev. Biochem.* **74**, 791–831.
2. Cronan, J. E., Jr & Gelmann, E. P. (1975). Physical properties of membrane lipids: biological relevance and regulation. *Bacteriol. Rev.* **39**, 232–256.
3. Hoang, T. T. & Schweizer, H. P. (1997). Fatty acid biosynthesis in *Pseudomonas aeruginosa*: cloning and characterization of the *fabAB* operon encoding β-hydroxyacyl-acyl carrier protein dehydratase (FabA) and β-ketoacyl-acyl carrier protein synthase I (FabB). *J. Bacteriol.* **179**, 5326–5332.
4. Zhu, K., Choi, K. H., Schweizer, H. P., Rock, C. O. & Zhang, Y. M. (2006). Two aerobic pathways for the formation of unsaturated fatty acids in *Pseudomonas aeruginosa*. *Mol. Microbiol.* **60**, 260–273.
5. Kimber, M. S., Martin, F., Lu, Y., Houston, S., Vedadi, M., Dharamsi, A. *et al.* (2004). The structure of (3*R*)-hydroxyacyl-acyl carrier protein dehydratase (FabZ) from *Pseudomonas aeruginosa*. *J. Biol. Chem.* **279**, 52593–52602.
6. Lu, Y. J., White, S. W. & Rock, C. O. (2005). Domain swapping between *Enterococcus faecalis* FabN and FabZ proteins localizes the structural determinants for isomerase activity. *J. Biol. Chem.* **280**, 30342–30348.
7. Leesong, M., Henderson, B. S., Gillig, J. R., Schwab, J. M. & Smith, J. L. (1996). Structure of a dehydratase-isomerase from the bacterial pathway for biosynthesis of unsaturated fatty acids: two catalytic activities in one active site. *Structure*, **4**, 253–264.
8. Campbell, J. W. & Cronan, J. E., Jr. (2001). Bacterial fatty acid biosynthesis: targets for antibacterial drug discovery. *Annu. Rev. Microbiol.* **55**, 305–332.
9. Heath, R. J., White, S. W. & Rock, C. O. (2002). Inhibitors of fatty acid synthesis as antimicrobial chemotherapeutics. *Appl. Microbiol. Biotechnol.* **58**, 695–703.
10. Parsons, J. B. & Rock, C. O. (2011). Is bacterial fatty acid synthesis a valid target for antibacterial drug discovery? *Curr. Opin. Microbiol.* **14**, 544–549.
11. Rees, D. C., Congreve, M., Murray, C. W. & Carr, R. (2004). Fragment-based lead discovery. *Nat. Rev., Drug Discov.* **3**, 660–672.
12. Carr, R. A., Congreve, M., Murray, C. W. & Rees, D. C. (2005). Fragment-based lead discovery: leads by design. *Drug Discovery Today*, **10**, 987–992.
13. Krissinel, E. & Henrick, K. (2007). Inference of macromolecular assemblies from crystalline state. *J. Mol. Biol.* **372**, 774–797.
14. Brinster, S., Lamberet, G., Staels, B., Trieu-Cuot, P., Gruss, A. & Poyart, C. (2009). Type II fatty acid synthesis is not a suitable antibiotic target for Gram-positive pathogens. *Nature*, **458**, 83–86.
15. He, L., Zhang, L., Liu, X., Li, X., Zheng, M., Li, H. *et al.* (2009). Discovering potent inhibitors against the β-hydroxyacyl-acyl carrier protein dehydratase (FabZ) of *Helicobacter pylori*: structure-based design, synthesis, bioassay, and crystal structure determination. *J. Med. Chem.* **52**, 2465–2481.
16. Maity, K., Venkata, B. S., Kapoor, N., Surolia, N., Surolia, A. & Suguna, K. (2011). Structural basis for the functional and inhibitory mechanisms of β-hydroxyacyl-acyl carrier protein dehydratase (FabZ) of *Plasmodium falciparum*. *J. Struct. Biol.* **176**, 238–249.
17. Zhang, L., Liu, W., Hu, T., Du, L., Luo, C., Chen, K. *et al.* (2008). Structural basis for catalytic and inhibitory mechanisms of β-hydroxyacyl-acyl carrier protein dehydratase (FabZ). *J. Biol. Chem.* **283**, 5370–5379.
18. Zhang, L., Kong, Y., Wu, D., Zhang, H., Wu, J., Chen, J. *et al.* (2008). Three flavonoids targeting the β-hydroxyacyl-acyl carrier protein dehydratase from *Helicobacter pylori*: crystal structure characterization with enzymatic inhibition assay. *Protein Sci.* **17**, 1971–1978.
19. Kong, Y. H., Zhang, L., Yang, Z. Y., Han, C., Hu, L. H., Jiang, H. L. & Shen, X. (2008). Natural product juglone targets three key enzymes from *Helicobacter pylori*: inhibition assay with crystal structure characterization. *Acta Pharmacol. Sin.* **29**, 870–876.
20. Schwab, J. M. & Klassen, J. B. (1984). Steric course of the allylic rearrangement catalyzed by β-hydroxydecanoylthioester dehydrase—mechanistic implications. *J. Am. Chem. Soc.* **106**, 7217–7227.

21. Lapeyre, C., Delomenede, M., Bedos-Belval, F., Duran, H., Negre-Salvayre, A. & Baltas, M. (2005). Design, synthesis, and evaluation of pharmacological properties of cinnamic derivatives as antiatherogenic agents. *J. Med. Chem.* **48**, 8115–8124.
22. Kim, M. I., Kwon, S. J. & Dordick, J. S. (2009). In vitro precursor-directed synthesis of polyketide analogues with coenzyme a regeneration for the development of antiangiogenic agents. *Org. Lett.* **11**, 3806–3809.
23. Oke, M., Carter, L. G., Johnson, K. A., Liu, H., McMahon, S. A., Yan, X. *et al.* (2010). The Scottish Structural Proteomics Facility: targets, methods and outputs. *J. Struct. Funct. Genomics*, **11**, 167–180.
24. Liu, H. & Naismith, J. H. (2008). An efficient one-step site-directed deletion, insertion, single and multiple-site plasmid mutagenesis protocol. *BMC Biotechnol.* **8**, 91.
25. Studier, F. W. (2005). Protein production by auto-induction in high density shaking cultures. *Protein Expression Purif.* **41**, 207–234.
26. Meyer, B. & Peters, T. (2003). NMR spectroscopy techniques for screening and identifying ligand binding to protein receptors. *Angew. Chem.* **42**, 864–890.
27. Dalvit, C., Pevarello, P., Tato, M., Veronesi, M., Vulpetti, A. & Sundstrom, M. (2000). Identification of compounds with binding affinity to proteins via magnetization transfer from bulk water. *J. Biomol. NMR*, **18**, 65–68.
28. Otwinowski, Z. & Minor, W. (1997). Processing of X-ray diffraction data collected in oscillation mode. *Methods Enzymol.* **276**, 307–326.
29. Winter, G. (2010). Xia2: an expert system for macromolecular crystallography data reduction. *J. Appl. Crystallogr.* **43**, 186–190.
30. Zhang, Z., Sauter, N. K., van den Bedem, H., Snell, G. & Deacon, A. M. (2006). Automated diffraction image analysis and spot searching for high-throughput crystal screening. *J. Appl. Crystallogr.* **39**, 112–119.
31. Sauter, N. K., Grosse-Kunstleve, R. W. & Adams, P. D. (2004). Robust indexing for automatic data collection. *J. Appl. Crystallogr.* **37**, 399–409.
32. Kabsch, W. (1993). Automatic processing of rotation diffraction data from crystals of initially unknown symmetry and cell constants. *J. Appl. Crystallogr.* **26**, 795–800.
33. Evans, P. (2006). Scaling and assessment of data quality. *Acta Crystallogr., Sect. D: Biol. Crystallogr.* **62**, 72–82.
34. Vagin, A. & Teplyakov, A. (1997). MOLREP: an automated program for molecular replacement. *J. Appl. Crystallogr.* **30**, 1022–1025.
35. McCoy, A. J., Grosse-Kunstleve, R. W., Adams, P. D., Winn, M. D., Storoni, L. C. & Read, R. J. (2007). Phaser crystallographic software. *J. Appl. Crystallogr.* **40**, 658–674.
36. Adams, P. D., Afonine, P. V., Bunkoczi, G., Chen, V. B., Davis, I. W., Echols, N. *et al.* (2010). PHENIX: a comprehensive Python-based system for macromolecular structure solution. *Acta Crystallogr., Sect. D: Biol. Crystallogr.* **66**, 213–221.
37. Emsley, P. & Cowtan, K. (2004). Coot: model-building tools for molecular graphics. *Acta Crystallogr., Sect. D: Biol. Crystallogr.* **60**, 2126–2132.
38. Murshudov, G. N., Vagin, A. A. & Dodson, E. J. (1997). Refinement of macromolecular structures by the maximum-likelihood method. *Acta Crystallogr., Sect. D: Biol. Crystallogr.* **53**, 240–255.
39. Schuttelkopf, A. W. & van Aalten, D. M. (2004). PRODRG: a tool for high-throughput crystallography of protein–ligand complexes. *Acta Crystallogr., Sect. D: Biol. Crystallogr.* **60**, 1355–1363.
40. Chen, V. B., Arendall, W. B., 3rd, Headd, J. J., Keedy, D. A., Immormino, R. M., Kapral, G. J. *et al.* (2010). MolProbity: all-atom structure validation for macromolecular crystallography. *Acta Crystallogr., Sect. D: Biol. Crystallogr.* **66**, 12–21.
41. Schrodinger, LLC. (2010). The PyMOL Molecular Graphics System, Version 1.3r1.
42. Kass, L. R. (1969). β-Hydroxydecanoyl thioester dehydrase from *Escherichia coli*. *Methods Enzymol.* **14**, 73–80.